
SOLIDS
AND LIQUIDS

Ab Initio Study of the Relation between the Structural, Magnetic, and Optical Properties of Normal and Inverse MnGa_2O_4 Spinels

V. S. Zhandun^{a,*} and A. V. Nemtsev^a

^a Kirensky Institute of Physics Federal Research Center “Krasnoyarsk Science Centre,” Siberian Branch,
Russian Academy of Sciences, Krasnoyarsk, 660036 Russia

*e-mail: jvc@iph.krasn.ru

Received May 28, 2019; revised July 25, 2019; accepted October 15, 2019

Abstract—The electronic, magnetic, and optical properties of MnGa_2O_4 in the structure of the normal and inverse spinels are subjected to an ab initio investigation and comparison. The generalized gradient approximation (GGA) predicts that the normal MnGa_2O_4 spinel is a semiconductor with a bandgap of about 0.7 eV, and a bandgap in the structure of the inverse spinel appears only in terms of the GGA + U approach. A simple exchange interaction model is used to calculate exchange integrals. In both structure types, MnGa_2O_4 exhibits antiferromagnetic behavior, and the normal structure is energetically favorable. The inverse spinel becomes energetically favorable only when a negative pressure is applied. The absorption spectra of the normal spinel are found to have a spectral window at a wavelength larger than 450 nm.

DOI: 10.1134/S106377612002017X

1. INTRODUCTION

Manganese-containing oxides with a spinel structure attract close attention from both fundamental and applied standpoints due to a wide spectrum of their physicochemical properties [1–4]. The properties of spinels can change as functions of their crystal structure and chemical composition. Spinels can exist in the following two structural modifications: normal and inverse spinels. The chemical formula of a normal spinel can be written as AB_2O_4 , where A and B tetrahedrally and octahedrally coordinated cations, respectively. In an inverse spinel, the location of cations is alternative: A cations and half of B cations exchange their sites. Inverse spinels have the chemical formula B(AB)O_4 , A cations and half of B cations occupy octahedral sites and the other half of B cations is retained in tetrahedral sites. In this work, we perform an ab initio investigation of the magnetic, electronic, and optical properties of the MnGa_2O_4 oxide. MnGa_2O_4 has the structure of cubic AB_2O_4 spinel, where tetrahedral sites (A) are occupied by Mn^{2+} ions and octahedral sites (B) are occupied by Ga^{3+} ions. Neutron powder diffraction showed that the spin moments at the ions located at sites A are antiferromagnetically coupled at low temperatures, and the Néel temperature of the antiferromagnetic transition is $T_N = 33$ K [5]. Although manganese-containing spinels are being extensively studied, the information on the properties of the MnGa_2O_4 spinel is scarce [5–8], and there are no ab initio theoretical investigations of

the properties of bulk MnGa_2O_4 . Therefore, the purpose of this work is to theoretically analyze the structural, electronic, magnetic, and optical properties of MnGa_2O_4 in its normal and inverse structures in terms of an ab initio approach and various approximations. The structure of this work is as follows. In Section 2, we briefly describe calculation details. In Section 3, the magnetic, electronic, and optical properties of the normal and inverse MnGa_2O_4 spinels are compared, and conclusions are drawn in Section 4.

2. CALCULATION TECHNIQUE

All ab initio calculations were carried out using the VASP software package [9] and the PAW (projector augmented wave) pseudopotentials [10, 11]. For Mn, Ga, and O atoms, we used the valence electron configurations $3d^7 4s^2$, $3d^{10} 4s^2 4p^1$, and $3s^2 3p^4$, respectively. The calculations were based on the density functional theory, where the exchange–correlation potential was used in the PBE (Perdew–Burke–Ernzerhof) parameterization [12] and the generalized gradient approximation (GGA). A plane wave cutoff energy of 500 eV was used for all calculations. Integration over the Brillouin zone was performed on a $8 \times 8 \times 8$ Monkhorst–Pack grid [13]. The GGA + U approach were performed in Dudarev’s approximation [14] at $U = 5$ eV for the Mn ion (according to [15]).

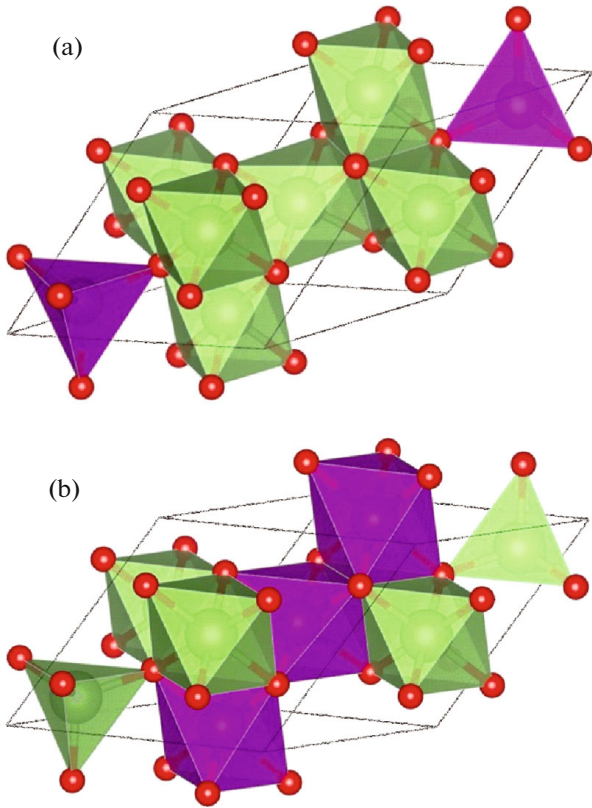


Fig. 1. (Color online) Unit cells of (a) normal and (b) inverse MnGa_2O_4 spinels. The local environment of Mn ions is purple and the local environment of Ga ions is green.

3. RESULTS AND DISCUSSION

Figure 1 shows the structures of the normal and inverse MnGa_2O_4 spinels. In all calculations, we used a rhombohedral unit cell containing two Mn ions, four Ga ions, and eight oxygen ions. Manganese atoms in the structure of the normal spinel are in the tetrahedral environment of oxygen atoms, and Ga atoms are surrounded by six oxygen ions located at the vertices of an octahedron. Manganese atoms in the structure of the inverse spinel are at the center of an octahedron formed by oxygen atoms, and Ga atoms are located at the centers of both oxygen tetrahedra and oxygen octahedra. Therefore, the magnetic atoms in the normal and inverse structures have different local environment, namely, tetrahedral and octahedral environ-

Table 1. Total energy for ferromagnetic (FM) and antiferromagnetic (AFM) ordering of magnetic moments

Magnetic ordering	E , eV	
	normal spinel	inverse spinel
FM	-94.48	-93.51
AFM	-94.56	-93.66

ment, respectively. The structural geometry was fully optimized in terms of the GGA approach. The calculated optimized lattice parameters of MnGa_2O_4 in the structures of the normal ($a = 8.51 \text{ \AA}$) and inverse ($a = 8.55 \text{ \AA}$) spinels are close to the experimental lattice parameter ($a = 8.43 \text{ \AA}$) [16]. We also estimated the Mn–O bond length: $d_{\text{Mn-O}} = 2.03 \text{ \AA}$ and $d_{\text{Mn-O}} = 2.11 \text{ \AA}$ for the normal and inverse spinels, respectively. The distances inside the MnO_6 octahedron are seen to be larger than those in the MnO_4 tetrahedron.

As an initial step, we calculate the energy of the ground magnetic state of MnGa_2O_4 for both structures. As is seen from Table 1, an antiferromagnetic state is energetically more favorable than a ferromagnetic state for both types of structures. Moreover, we found that the MnGa_2O_4 spinel in the structure of inverse spinel is energetically less favorable than that in the structure of normal spinel. In the ground magnetic state, the magnetic moments at Mn ions are antiferromagnetically ordered and have an absolute value $\mu = 4.35\mu_B$ ($\mu = 4.58\mu_B(\text{GGA} + U)$), where μ_B is the Bohr magneton.

In the normal MnGa_2O_4 spinel, the indirect exchange between the tetrahedrally coordinated Mn^{2+} ions occurs via intermediate gallium B cations. In the inverse MnGa_2O_4 spinel, the indirect exchange between the octahedrally coordinated Mn^{2+} ions occurs via intermediate gallium A and B cations. To estimate the indirect exchange interactions in a MnGa_2O_4 crystal, we used the simple indirect interaction model [17], which is based on the theory of indirect exchange interaction [18, 19]. In terms of exchange interaction, the structure of the crystal is characterized by the following indirect exchange integrals with allowance for the filling of some cation orbitals and the symmetries of the exchange interaction lattice J_{ij} , where i and j are the numbers of non-equivalent crystallographic sites for magnetic ions,

$$J_{AA} = -\frac{2}{25}\alpha(U + V), \quad \alpha = \frac{432}{7}\alpha^2\left(\frac{8}{9}b^2 + c^2\right),$$

$$V = \sum_i n_{\text{Bi}}U_{\text{Bi}}, \quad J_{BB} = -\frac{4}{75}c(8b + 3c)U,$$

where $U(\text{Mn}^{2+}) = 7 \text{ eV}$ is the excitation energy of the cation ligand; a , b , and c are the electron transfer parameters, which are the squared coefficients of mixing of ligand cations A and B for the σ and π bonds ($a = 0.08$, $b = 0.02$, $c = 0.01$), respectively; and n_{Bi} and U_{Bi} are the concentration and the excitation energy of the intermediate B cations [17–19]. The calculated exchange integrals are $J_{\text{Mn-Mn}} = -0.53 \text{ meV}$ (6.15 K) and $J_{\text{Mn-Mn}} = -0.71 \text{ meV}$ (8.24 K) for the normal and inverse spinels, respectively. The indirect exchange interaction integrals in both structures are seen to be antiferromagnetic according to the results of our ab initio calculations and the experimental data from [5].

Note also that both Mn–Mn exchange integrals are small, which provides the experimentally detected low Néel temperature.

Figure 2 shows the calculated total and partial densities of states and the band structure of MnGa_2O_4 in the normal spinel structure in terms of the GGA and GGA + U approximations. The bands were classified according to their symmetries at the Γ point of the Brillouin zone. The maxima of the valence band and the minima of the conduction band are located at the Γ point of the Brillouin zone. The filled band nearest to the Fermi level (Fig. 2b, $T2g$) is formed by the $t2g$ states of Mn ions with a small impurity of the p states of O atoms at the boundary points of the Brillouin zone. The first empty band ($A1g$) is formed by the s states of Ga^{3+} ions. The normal MnGa_2O_4 spinel is seen to have a bandgap of about 0.7 eV and GGA + U increases it to 1.7 eV. The bandgap in the major part of the Brillouin zone is about 2.5 eV, and it narrows to 0.7 eV in the vicinity of the Γ point because of the dispersion features of the broad s conduction band. It should be noted that the empty d states are at a distance of 2 eV from the Fermi energy (Fig. 2c). The valence and empty $t2g$ and eg states are in the ranges $[-1.5, 0]$ eV and $[2.0, 3.5]$ eV, respectively, near the Fermi energy. The spin-up states are filled with d electrons and the spin-down states are empty; that is, the manganese ion is in a high-spin state. It should be noted that Hubbard potential U most strongly affects the conduction bands, which undergo a string Fermi-energy-induced shift. The p states of the oxygen ion, which are delocalized over a wide energy range $[-5, -2]$ eV, also shift toward the Fermi energy. It is interesting that Hubbard potential U more strongly affects the delocalized electronic states, which can point to the absence of strong electronic correlations in the compound under study [20].

As for the inverse spinel, a small bandgap appears only in the GGA + U calculation (Figs. 3a, 3b). In contrast to the band structure of the normal spinel, the broad s band ($A1g$) in the inverse spinel lies below the Fermi energy, which leads to the closure of the bandgap (see Fig. 3b). Therefore, it is the s electrons of Ga that cause metallic behavior in the inverse MnGa_2O_4 spinel. The d states of the Mn ion are in the energy range characteristic of the normal structure, and the manganese ion is also in a high-spin state. However, as a result of the octahedral environment of Mn ions, the $t2g$ and eg states exchange places in comparison with the density of states in the normal spinel (Fig. 3c). It should be noted that the large distance between atoms in the inverse spinel, which was noted above, can lead to a more pronounced electron delocalization and, hence, a stronger tendency toward the formation of metallic behavior in the inverse spinel. The influence of Hubbard potential U is similar to that in the normal spinel: the broad s band moves from the Fermi energy and opens up a gap. Here, the influence of Hubbard

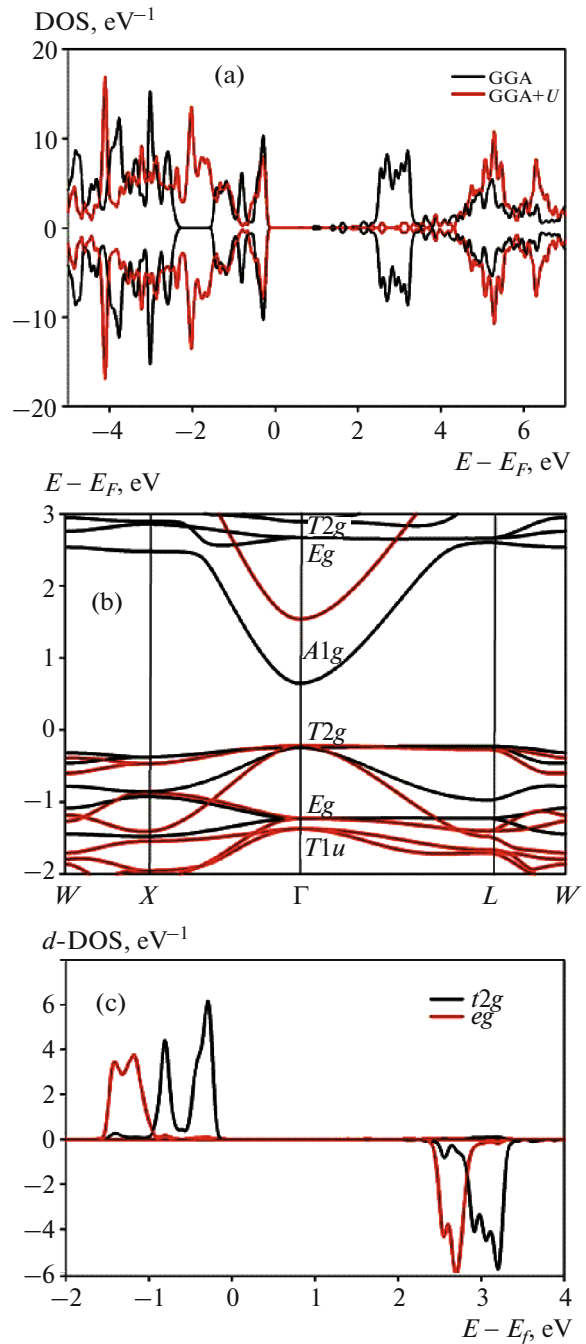


Fig. 2. (Color online) Normal spinel structure. (a) Total density of states (DOS) for MnGa_2O_4 in (black line) GGA and (red line) GGA + U approximation; negative values of DOS correspond to spin-down states. (b) Band structure of MnGa_2O_4 calculated using (black line) GGA and (red line) GGA + U approximation. (c) Partial densities of electronic d states (d -DOS) for Mn^{2+} ions in MnGa_2O_4 . (black lines) $t2g$ states and (red line) eg states. Zero in the energy axis corresponds to the Fermi energy.

potential U on the conduction bands is stronger than on the valence bands.

As noted above, the inverse spinel is energetically less favorable as compared to the normal spinel at zero

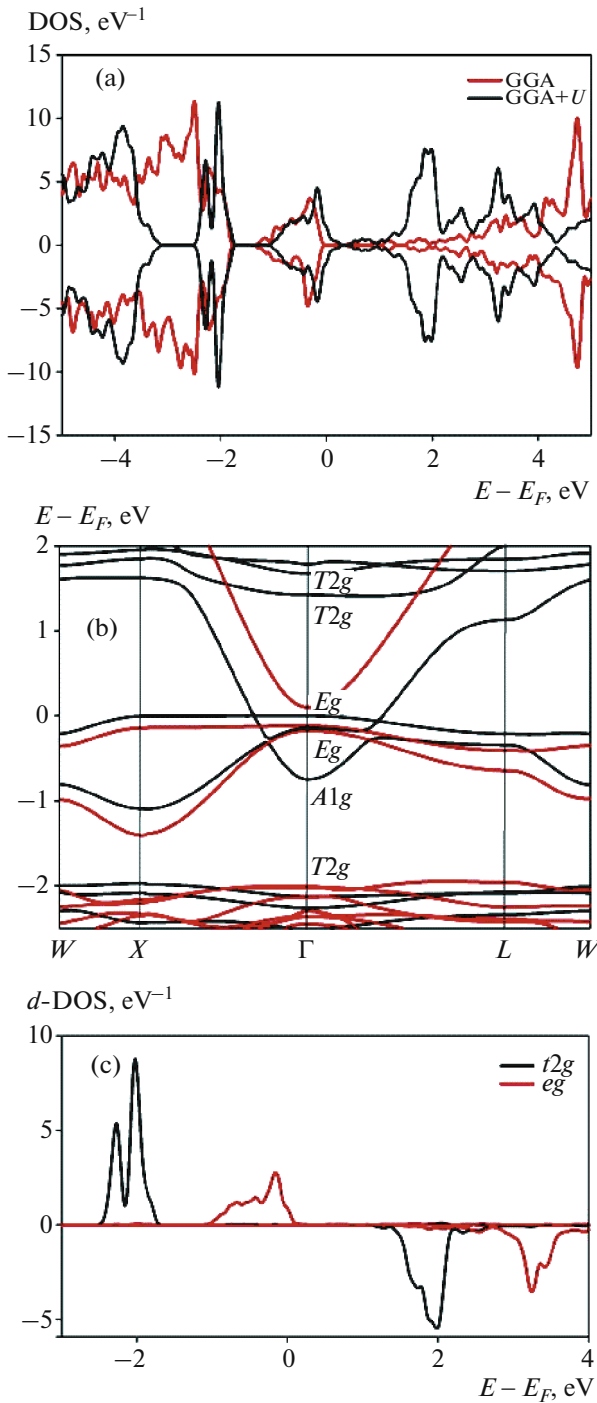


Fig. 3. (Color online) The same as in Fig. 2 for the inverse spinel structure.

pressure and temperature. However, the application of pressure can bring about the conditions that promote the formation of the inverse spinel structure during growth. To study this possibility, we calculated the change in the enthalpies of the normal and inverse spinels at a negative pressure (expansion/increase in volume). As is seen in Fig. 4, the normal spinel still has a

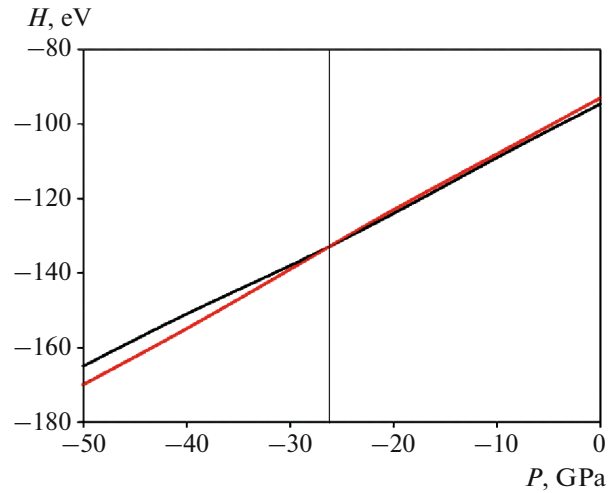


Fig. 4. (Color online) Optical absorption spectra of MnGa_2O_4 in the structures of (black curve) normal and (red curve) inverse spinel.

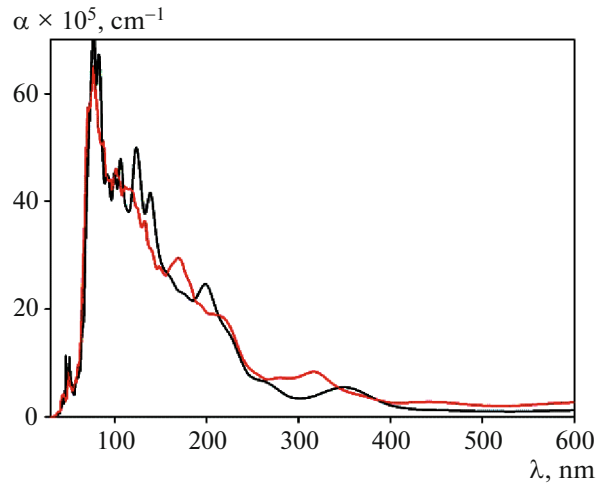


Fig. 5. Enthalpy vs. hydrostatic pressure for (black curve) normal and (red curve) inverse spinel.

lower energy at a low pressure. However, an increase in the negative pressure induces a transition between the two structures at $P = -27$ GPa. A further increase in the pressure stabilizes the structure of the inverse spinel instead of the normal spinel. Therefore, the inverse structure is thought to be energetically favorable at $P > -27$ GPa.

In Fig. 5, we compare the wavelength dependences of the absorption coefficients of the normal and inverse MnGa_2O_4 spinels. Both absorption spectra are seen to have the same shape and behavior. Both absorption coefficients have a high peak in the range [500, 300] nm. An analysis of the electronic structure demonstrates that the main contribution to the absorption peak is made by the electron transitions

from the filled d bands of Mn, which are located at low energies, to the empty d (Mn) and s (Ga) bands (see Figs. 2b, 3b). The low peak at 320–350 nm is also caused by the transition between the d states of the Mn^{2+} ion. The spectral window in the normal spinel at $\lambda > 400$ nm is related to the presence of a bandgap. Although the absorption coefficient in the inverse spinel is significantly lower in the same range, it is still nonzero because of the metallic nature of the inverse spinel.

4. CONCLUSIONS

The magnetic, electronic, and optical properties of the antiferromagnetic MnGa_2O_4 spinel were calculated for the following two structure types: the normal and inverse spinels. In both structures, the compound is antiferromagnetic with magnetic moments $\mu = 4.35\mu_B$ at ions. The calculated exchange integrals are small, which explains the experimentally detected low Néel temperature. The inverse spinel is less energetically favorable than the normal spinel. However, the application of a negative pressure makes the inverse spinel energetically favorable in comparison with the normal spinel.

The calculation of MnGa_2O_4 in the normal spinel structure exhibits a bandgap of about 0.7 eV. A small bandgap in the inverse spinel structure appears only when Hubbard potential U is taken into account. The valence bands near the Fermi level are formed by the t_{2g} and e_g electrons of Mn in the normal and inverse spinels, respectively. The conduction band near the Fermi energy is formed by the empty s states of Ga.

The optical spectra of both structures that were obtained in ab initio calculations were found to have similar shape and behavior. The normal MnGa_2O_4 spinel has a high absorption peak in the range [50–300] nm and a broad spectral window at $\lambda > 450$ nm. The d – s and d – d transitions mainly contribute to the absorption.

FUNDING

The reported study was funded by Russian Foundation for Basic Research, Government of Krasnoyarsk Territory, Krasnoyarsk Regional Fund of Science to the research project no. 18-42-243019: “First-principles studies of the polarization, magnetic, electronic, and magnetoelectric properties of functional compounds with a spinel structure containing 3d and 4f ions.”

The calculations were performed with the computer resources of “Complex modeling and data processing research installations of mega-class” SRC “Kurchatovsky Institute” (<http://ckp.urki.ru>).

REFERENCES

1. N. Tristan, J. Hemberger, A. Krimmel, H. A. Krug von Nidda, V. Tsurkan, and A. Loidl, *Phys. Rev. B* **72**, 174404 (2005).
2. S.-H. Lee, H. Takagi, D. Louca, M. Matsuda, S. Ji, H. Ueda, Y. Ueda, T. Katsufuji, J.-H. Chung, S. Park, S.-W. Cheong, and C. Broholm, *J. Phys. Soc. Jpn.* **79**, 0110041 (2010).
3. M. F. Bekheet, G. Miehe, C. Fasel, A. Gurlo, and R. Riedel, *Dalton Trans.* **41**, 3374 (2012).
4. M. F. Bekheet, L. Dubrovinsky, and A. Gurlo, *J. Solid State Chem.* **230**, 301 (2015).
5. B. Boucher, A. G. Herpin, and A. Oles, *J. Appl. Phys.* **37**, 960 (1966).
6. P. G. Casado and I. Rasines, *Z. Kristallogr.* **160**, 33 (1982).
7. Jin Young Lee, Dae Sung Kim, Chan Woong Na, and Jeunghye Park, *J. Phys. Chem. C* **111**, 12207 (2007).
8. O. S. Venediktova, O. A. Bulavchenko, T. N. Afonasenkov, P. G. Tsyul'nikov, Z. S. Vinokurov, Yu. A. Chesalov, and S. V. Tsybulya, *J. Alloys Compd.* **725**, 496 (2017).
9. G. Kresse and J. Furthmüller, *Phys. Rev. B* **54**, 11169 (1996).
10. P. E. Blochl, *Phys. Rev. B* **50**, 17953 (1994).
11. G. Kresse and D. Joubert, *Phys. Rev. B* **59**, 1758 (1999).
12. J. P. Perdew, K. Burke, and M. Ernzerhof, *Phys. Rev. Lett.* **77**, 3865 (1996).
13. H. J. Monkhorst and J. D. Pack, *Phys. Rev. B* **13**, 5188 (1976).
14. S. L. Dudarev, G. A. Botton, S. Y. Savrasov, C. J. Humphreys, and A. P. Sutton, *Phys. Rev. B* **57**, 1505 (1998).
15. E. Şaştoğlu, C. Friedrich, and S. Blügel, *Phys. Rev. B* **83**, 121101(R) (2011).
16. M. Lensen and A. Michel, *C. R. (Paris)* **246**, 2766 (1958).
17. O. A. Bayukov and A. F. Savitskii, *Phys. Solid State* **36**, 1049 (1994).
18. P. W. Anderson, *Phys. Rev.* **115**, 2 (1959).
19. G. A. Sawatzky, W. Geertsma, and C. Haas, *J. Magn. Magn. Mater.* **3**, 37 (1976).
20. I. Sandalov, N. Zamkova, V. Zhandun, I. Tarasov, S. Varnakov, I. Yakovlev, L. Solovyov, and S. Ovchinnikov, *Phys. Rev. B* **92**, 205129 (2015).

Translated by K. Shakhlevich